A Practical Validation of RIS Detection and Identification

Recep Vural, Aymen Khaleel, *Member, IEEE*, Majid Gerami, and Ertugrul Basar, *Fellow, IEEE*

Abstract—Reconfigurable intelligent surface (RIS)-assisted communication is a key enabling technology for next-generation wireless communication networks, allowing for the reshaping of wireless channels without requiring traditional radio frequency (RF) active components. While their passive nature makes RISs highly attractive, it also presents a challenge: RISs cannot actively identify themselves to user equipments (UEs). Recently, a new method has been proposed to detect and identify RISs by letting them modulate their identities in the signals reflected from their surfaces. In this letter, we first propose a new and simpler modulation method for RISs and then validate the concept of RIS detection and identification (RIS-ID) using a real-world experimental setup. The obtained results validate the RIS-ID concept and show the effectiveness of our proposed modulation method over different operating scenarios and systems settings.

Index Terms—Reconfigurable intelligent surfaces, practical implementation, detection, identification.

I. INTRODUCTION

RECONFIGURABLE intelligent surfaces (RISs), composed of large arrays of controllable elements, have emerged as an enabling technology for next-generation wireless communication systems, particularly in the context of 6G networks. By controlling the amplitude, phase, and polarization of the signals hitting their surfaces, RISs reshape the propagation environment and bring several advantages, such as extended coverage, enhanced data rates, and increased energy efficiency [1]. Moreover, RISs can facilitate better interference management [2], provide robust security through signal manipulation [3], and enable precise localization for user equipment (UE) by altering the signal propagation paths [4].

While RISs are commonly used as passive beamforming arrays in wireless systems to control the propagation environment, several works have explored their potential to be used as an over-the-air modulator in wireless transmission systems [5]. In [6], an RIS-based 8-PSK transmitter for single-input-single-output (SISO) transmission is proposed, which modulates the incident signal by controlling the phase response of the RIS elements. This approach achieves data transmission at a rate of 6.144 Mb/s without the need for traditional RF components. The authors of [7] extended the idea to a multiple-input-multiple-output (MIMO) systems and developed an RIS-based

Recep Vural, Aymen Khaleel, and Ertugrul Basar are with the Communications Research and Innovation Laboratory (CoreLab), Department of Electrical and Electronics Engineering, Koç University, Sariyer, Istanbul, Turkey (e-mail: rvural22@ku.edu.tr; akhaleel@ku.edu.tr; ebasar@ku.edu.tr).

Majid Gerami is with Huawei Technologies Sweden AB, Lund, Sweden (email: majid.gerami@huawei.com).

RF chain-free 16-QAM transmitter, achieving a data rate of 20 Mb/s. Another notable application of RIS-based modulation is studied in [8], where RISs are utilized for UE localization. In this system, the base station (BS) transmits an unmodulated carrier signal, which is then modulated by multiple RISs at different time slots, with each RIS imparting a unique m-sequence. These distinct m-sequences enable the UE to differentiate received signals from different RISs. Finally, UE's location is estimated by applying time-difference-of-arrival (TDOA) method on the received signals.

However, existing studies often presume that UEs are informed about the presence of deployed RISs, which is a reasonable assumption when the network provides this information to the UE. Nevertheless, the existence of RISs nearby, reported to the UE by the network, does not guarantee the establishment of a communication link due to potential obstacles between the RIS and the UE [9]. Therefore, to use an RIS effectively, it is essential first to determine whether the RIS is reachable by the UE. To the best of the authors' knowledge, this problem was first addressed in the literature in [9], where the authors proposed a method called RIS-ID to enable UE to identify reachable RISs in its environment. The RIS-ID method utilizes binary phase shift keying (BPSK) modulation by leveraging phase changes at the RIS. This method allowed the embedding of unique phase shift reflection patterns (PSRPs) into the carrier signal impinging on the RIS surfaces, enabling the UE to detect and uniquely identify reachable RISs.

However, in [8], since the RIS detection process is performed before synchronization, reflected BPSK symbols are expected to be distorted due to time, frequency, and phase offsets at the UE side, negatively affecting the correlation amplitude. In this letter, we first propose a new modulation method that is less sensitive to synchronization issues, particularly phase and frequency offsets, by leveraging the phase-dependent amplitude variations associated with RIS elements to mimic amplitude shift keying (ASK) modulation. Second, we validate the RIS-ID concept in a real-world experimental setup using different operating scenarios and systems settings.

The remainder of the letter is organized as follows. Section II presents the system model used for the proposed method and the detection algorithm that was developed to determine RIS reachability. Section III outlines the experimental setup and implementation. Section IV provides the experimental results and performance evaluation. Finally, Section V concludes the letter.

II. SYSTEM MODEL

Here, we briefly introduce the RIS-ID concept and then provide the system model related to our proposed modulation method, as follows.

A. RIS Detection and Identification Method

As proposed in [9], the RIS-ID process involves the UE continuously transmitting an omnidirectional, unmodulated carrier signal while simultaneously receiving the echoes. Reachable RISs in the vicinity of the UE reflect this signal, modulating it with their unique PSRPs. The UE then correlates the received signal with locally generated versions of the PSRPs, and if the correlation exceeds a predefined threshold, the corresponding RIS is declared reachable.

B. Proposed Modulation Method

As illustrated in Fig. 1, a UE seeks to identify reachable RISs in the environment using the signals reflected from their surfaces. Each RIS has an ID number uniquely associated with an amplitude reflection pattern (ARP) selected from Walsh-Hadamard codes. In the identification process, UE transmits an unmodulated carrier signal $x = 1$ and simultaneously collects M symbols, where M denotes the length of the ARP symbols. In contrast to [9], where a unity amplitude reflection coefficient was assumed and BPSK modulation was used, in this system, reachable RISs modulate the signal hitting their surface according to their ARPs by changing the amplitude of the reflected signals, exploiting the amplitude-phase correlation in RIS elements [10].

Consider L possible reachable RISs in a wireless environment. Then, the m-th collected symbol at the UE can be given as [9]

$$
\begin{aligned}
y_m &= x \sum_{l=1}^{L} \left[(\mathbf{h}_m^{(l)})^T \boldsymbol{\Phi}_m^{(l)} \mathbf{h}_m^{(l)} \right] \mu^{(l)} + n_m \\
&\stackrel{\mathrm{I}}{=} x \sum_{l=1}^{L} a_m^{(l)} e^{j\phi_m^{(l)}} \left[(\mathbf{h}_m^{(l)})^T \mathbb{I}_{N^{(l)}} \mathbf{h}_m^{(l)} \right] \mu^{(l)} + n_m \\
&\stackrel{\mathrm{II}}{=} \sum_{l=1}^{L} a_m^{(l)} e^{j\phi_m^{(l)}} \tilde{h}^{(l)} \mu^{(l)} + n_m
\end{aligned}
\tag{1}
$$

where $n_m \sim \mathcal{N}_{\mathbb{C}}(0, \sigma_n^2)$ is the additive white Gaussian noise (AWGN) sample; $\mathbf{h}_{\mathrm{UR},m}^{(l)} \in \mathbb{C}^{N^{(l)}}$ and $\mathbf{h}_{\mathrm{RU},m}^{(l)} \in \mathbb{C}^{N^{(l)}}$ are UE-RIS and RIS-UE channel vectors, respectively, with l denoting the RIS index and $N^{(l)}$ representing the size of the l-th RIS; $\boldsymbol{\Phi}_m^{(l)}$ denotes the RIS phase shift matrix; $\mu^{(l)} \in \{0, 1\}$ represents the reachability of the RIS, where $\mu^{(l)} = 1$ indicates l-th RIS is reachable, and $\mu^{(l)} = 0$ indicates l-th RIS is unreachable. In step I, taking into account the ARP, we set $\boldsymbol{\Phi}_m^{(l)} = a_m^{(l)} e^{j\phi_m^{(l)}} \mathbb{I}_{N^{(l)}}$ where $\mathbb{I}_{N^{(l)}}$ is the identity matrix of size $N^{(l)}$, $\phi_m^{(l)}$ is the phase shift applied by RIS elements and $a_m^{(l)}$ is its amplitude coefficient (which depends on $\phi_m^{(l)}$). The relationship between amplitude coefficient a and phase ϕ can be given as [10]

$$
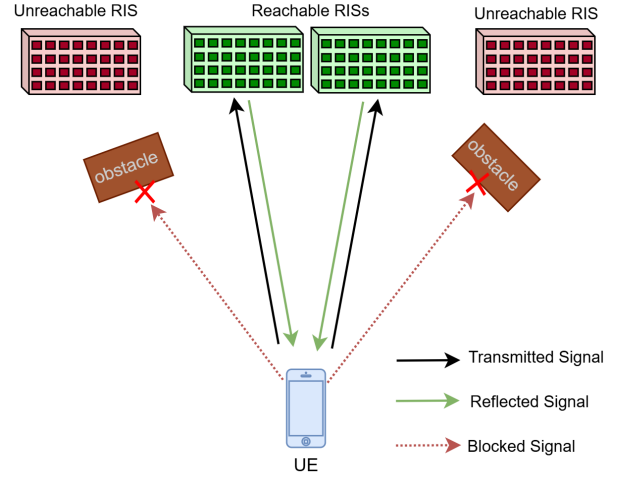a(\phi) = (1 - a_{\min}) \left(\frac{\sin(\phi - \delta) + 1}{2} \right)^{\gamma} + a_{\min}, \tag{2}
$$

Fig. 1. A UE aims to identify nearby reachable RISs.

where $a_{\min} \geq 0$, $\delta \geq 0$, and $\gamma \geq 0$ are the constants related to the specific circuit implementation.[1] $a_{\min}$ is the minimum amplitude coefficient, δ is the horizontal distance between $-\pi/2$ and $a_{\min}$, and γ controls the steepness of the function curve [10]. The RIS elements can apply two distinct phase shifts in our experimental setup, which will be detailed in Section III. Using (2), corresponding to these two phase shifts, $a_m^{(l)}$ can take on two values: $\hat{a}_1$ and $\hat{a}_2$.

Furthermore, in step II of (1), assuming that the channel coherence time exceeds the duration required to receive all reflected symbols at the UE, we eliminate the symbol index m and define $\tilde{h}^{(l)} = (\mathbf{h}^{(l)})^T \mathbb{I}_{N^{(l)}} \mathbf{h}^{(l)}$.

Considering (1) and (2), the amplitude of the received signal can be manipulated by changing $a_m^{(l)}$. Specifically, at the reflection of the m-th symbol, $a_m^{(l)}$ is defined as

$$
a_m^{(l)} = \begin{cases} \hat{a}_1, & q_{\tilde{m}}^{(l)} = 1 \\ \hat{a}_2, & q_{\tilde{m}}^{(l)} = -1 \end{cases}, \quad m, \tilde{m} \in \{1, 2, \ldots, M\}, \tag{3}
$$

where $q_{\tilde{m}}^{(l)} \in \{-1, 1\}$ is the $\tilde{m}$-th element of the ARP vector $\mathbf{q}^{(l)} = [q_1^{(l)}, \cdots, q_M^{(l)}]$ with $\tilde{m} = (c + m - 1) \mod M + 1$ denoting the index of the m-th ARP symbol modulating x. Here, c is the index of the first ARP symbol modulating x, modeled as a uniformly distributed random integer $c \in \mathcal{U}\{1, 2, \ldots, M-1\}$.

Consequently, the amplitude of the received vector $\mathbf{y} = [y_1, y_2, \ldots, y_M]$ relates to the cyclically shifted version of $\mathbf{q}^{(l)}$ from each reachable RIS. By quantifying these relationships, UE aims to detect reachable RISs in the environment.

The designed detection process is outlined in Algorithm 1, which takes as input l, $\mathbf{q}^{(l)}$, M, and a predefined detection threshold thr. The output is the reachability estimate of l-th RIS $\hat{\mu}^{(l)}$. The algorithm begins by obtaining the amplitude of the received signal and zero-centering it to obtain the required two distinct levels -1 and 1, creating the received symbols

---

[1]The model parameters $a_{\min}$, δ, and γ in (2) may vary from one RIS to another RIS due to the difference in the circuit implementation of the RIS elements. However, (2) serves as a general phase-dependent amplitude variations model.

Algorithm 1 RIS-ID Algorithm

Input: $l, \mathbf{q}^{(l)}, M, thr$
Output: $\widehat{\mu}^{(l)}$

1: Obtain the amplitude of the received signal and zero-center it to obtain $\tilde{\mathbf{y}} = [\tilde{y}_1, \tilde{y}_2, \ldots, \tilde{y}_M]$.
2: $D_{\max}^{(l)} \leftarrow 0$
3: **for** $i = 1$ to M **do**
4: $\quad \mathbf{q}_i^{(l)} \leftarrow \text{circshift}(\mathbf{q}^{(l)}, i)$: circular shift
5: $\quad d_i^{(l)} \leftarrow \frac{\mathbf{q}_i^{(l)} \cdot \tilde{\mathbf{y}}}{\sqrt{M}}$
6: $\quad D_i^{(l)} \leftarrow \left| d_i^{(l)} \right|^2$
7: $\quad$ **if** $D_i^{(l)} > D_{\max}^{(l)}$ **then**
8: $\quad\quad D_{\max}^{(l)} \leftarrow D_i^{(l)}$
9: $\quad$ **end if**
10: **end for**
11: **if** $D_{\max}^{(l)} > thr$ **then**
12: $\quad \widehat{\mu}^{(l)} \leftarrow 1$
13: **else**
14: $\quad \widehat{\mu}^{(l)} \leftarrow 0$
15: **end if**
16: **return** $\widehat{\mu}^{(l)}$

Fig. 2. The experiment setup to validate the RIS-ID scheme.

Fig. 3. The RIS hardware used in the experiment and the distribution of its elements between RIS 1 and RIS 2.

vector $\tilde{\mathbf{y}} = [\tilde{y}_1, \tilde{y}_2, \ldots, \tilde{y}_M]$. Next, the algorithm iteratively circularly shifts the ARP vector $\mathbf{q}^{(l)}$ by i positions, where i ranges from 1 to M. This shifting is necessary due to the unsynchronization between the RIS and UE, which causes the received signal to be modulated according to a cyclically shifted version of the ARP [9]. For each shift, the algorithm calculates $d_i^{(l)}$ by correlating the shifted ARP vector $\mathbf{q}_i^{(l)}$ with $\tilde{\mathbf{y}}$ and normalizes it by $\sqrt{M}$. The detection value $D_i^{(l)}$ is then obtained as the squared magnitude of $d_i^{(l)}$. The algorithm tracks the maximum detection value, $D_{\max}^{(l)}$, across all possible shifts and compares it with thr. If $D_{\max}^{(l)}$ exceeds thr, the RIS is considered reachable, and $\hat{\mu}^{(l)}$ is set to 1; otherwise, it is considered unreachable, and $\hat{\mu}^{(l)}$ is set to 0. By repeating Algorithm 1 for $l = 1, 2, \ldots, L$, the reachability estimate of each RIS is obtained.

As in [9], the performance of the proposed method can be assessed by false detection and miss detection probabilities. The false detection probability P_F indicates the probability of declaring an RIS is reachable while it is unreachable by UE. Conversely, the miss detection probability P_{miss} indicates the probability of declaration of an RIS as unreachable while it is reachable. These probabilities can be mathematically expressed as $P_F = P(\widehat{\mu}^{(l)} = 1 | \mu^{(l)} = 0)$ and $P_{\text{miss}} = P(\widehat{\mu}^{(l)} = 0 | \mu^{(l)} = 1)$.

III. EXPERIMENTAL SETUP AND IMPLEMENTATION

The measurement setup used in the experiment is shown in Fig. 2. The setup consists of an RIS hardware designed by Greenerwave and composed of 76 reflecting elements as shown in Fig. 3. Each element is equipped with two PIN diodes to control the phase shift applied to the incident signal in both vertical and horizontal polarization [11]. For the transmission and reception, ADALM-PLUTO software-defined radio (SDR) modules as well as horn antennas are
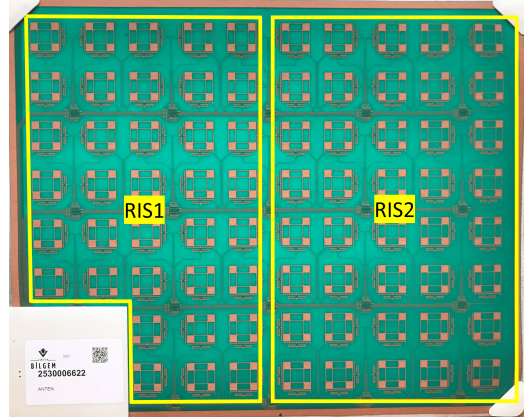
used. An unmodulated signal at a frequency of 5.27 GHz is transmitted from transmitter (Tx) SDR using a horn antenna directed at the RIS. The RIS is controlled by a computer to continuously change its phase shift matrix, creating unique ARPs. The signal reflected back from the RIS surface is received by the horn antenna of the receiver (Rx) SDR to be used in the detection process described in Algorithm 1.

In this experiment, we used two possibly reachable RISs ($L = 2$) in the environment: RIS 1 and RIS 2. Specifically, the experiment is carried out for the following scenarios: 'RIS 1 Reachable' ($\mu^{(1)} = 1$, $\mu^{(2)} = 0$), 'Both RISs Reachable' ($\mu^{(1)} = 1$, $\mu^{(2)} = 1$) and 'No RIS Reachable' ($\mu^{(1)} = 0$, $\mu^{(2)} = 0$). Due to the limitation of having only one RIS hardware available in our experimental setup, the 'Both RISs Reachable' scenario was realized by virtually partitioning the RIS into two separate segments, representing RIS 1 and RIS 2, as illustrated in Fig. 3. For each scenario, the experiment was performed under various settings of M and the Tx gain,[2] where 300 measurements are taken for each setting. The performance of the proposed method was then evaluated based on P_{miss}, P_F, and the average maximum detection value, $\overline{D}_{\max}^{(l)} = \frac{1}{300} \sum_{k=1}^{300} D_{\max,k}^{(l)}$, where k denotes the measurement index.

---

[2]Note that the ADALM-Pluto SDR does not provide a direct parameter for setting the Tx power. Instead, it offers control over the Tx gain, which serves as an indirect way for adjusting the output power.
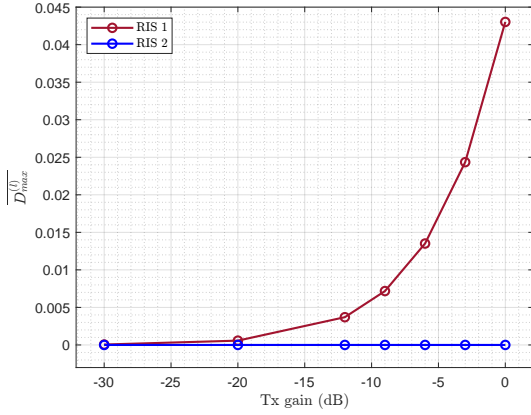
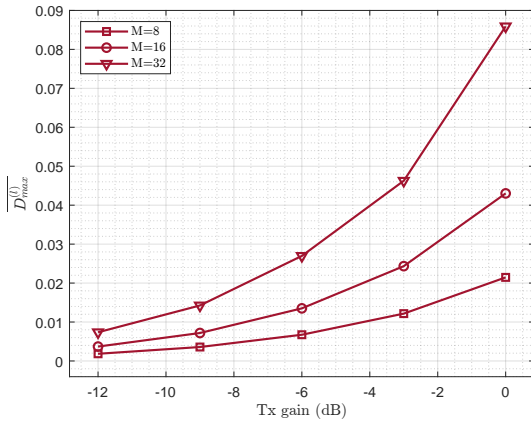Fig. 4. $\overline{D_{\max}^{(l)}}$ vs Tx gain for RIS 1 ($l = 1$) and RIS 2 ($l = 2$) in "RIS 1 Reachable" scenario.

Fig. 6. The effect of the Tx gain on P_{miss} of RIS 1 and P_F of RIS 2 in "RIS 1 Reachable" scenario.

Fig. 5. The effect of M on $\overline{D_{\max}^{(l)}}$ for RIS 1 in "RIS 1 Reachable" scenario.

Fig. 7. The effect of the Tx gain on $\overline{D_{\max}^{(l)}}$ for RIS 1 and RIS 2 in "Both RISs reachable" scenario.

IV. EXPERIMENTAL RESULTS

In this section, we provide experimental results to assess the performance of the practical RIS-ID method. In the experiments, unless otherwise specified, the code length is set as $M = 16$.

A. RIS 1 Reachable Scenario

In this scenario, all reflecting elements are assigned to RIS 1. Accordingly, the states of elements are adjusted according to the ARP of RIS 1. As seen in Fig. 4, when only RIS 1 is reachable, $\overline{D_{\max}^{(2)}}$ has low value and does not increase with the increase in Tx gain. On the other hand, $\overline{D_{\max}^{(1)}}$ is consistently higher than $\overline{D_{\max}^{(2)}}$, and increases with the Tx gain. For example, increasing the Tx gain by 3 dB approximately doubles $\overline{D_{\max}^{(1)}}$. Additionally, in Fig. 5, the effect of the ARP length M on $\overline{D_{\max}^{(1)}}$ is investigated. It can be seen that $\overline{D_{\max}^{(1)}}$ increases with the increase of M where doubling M increases the $\overline{D_{\max}^{(1)}}$ by a factor of two, due to the increase in the correlation amplitude.

In Fig. 6, the effect of the Tx gain on P_{miss} of RIS 1 and P_F of RIS 2 is examined, with the x-axis of the figure representing the normalized detection threshold $\widetilde{thr}$. Here, $\widetilde{thr} = thr/P_{noise}$, where P_{noise} is the noise power measured at the Rx SDR. From Fig. 6, it is observed that while increasing the Tx gain decreases P_{miss} of RIS 1, it

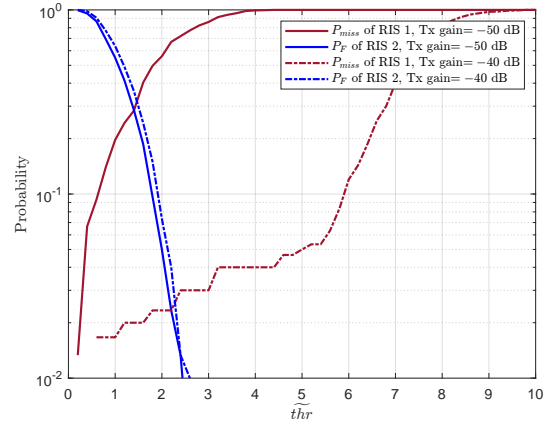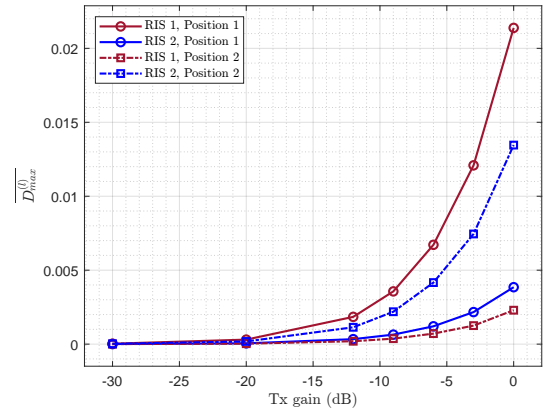does not affect P_F of RIS 2 considerably. Additionally, it is clearly seen that increasing $\widetilde{thr}$ decreases P_F of RIS 2 while increases P_{miss} of RIS 1 as expected [9].

B. Both RISs Reachable Scenario

In this scenario, while approximately half of reflecting elements are assigned to RIS 1, the other half are assigned to RIS 2 as seen in Fig. 3. Accordingly, the states of elements are adjusted based on their assignments: those assigned to RIS 1 are configured according to the ARP of RIS 1, while those assigned to RIS 2 are configured according to the ARP of RIS 2. Fig. 7 shows the effect of the Tx gain on $\overline{D_{\max}^{(l)}}$ for RIS 1 and RIS 2 when both RISs are reachable. The experiment is performed for two different positions of the UE. It is observed that while $\overline{D_{\max}^{(1)}}$ in position 1 compared to $\overline{D_{\max}^{(2)}}$, the opposite is true in position 2. This behaviour is resulted from that the transmitted signal can not be focused on both RISs fairly due to the miss alignment between the different components of the experiment. Additionally, it is seen that increasing the Tx gain increases $\overline{D_{\max}^{(l)}}$ for both RISs where increasing the Tx gain 3 dB leads to and approximately two-fold increase in $\overline{D_{\max}^{(l)}}$ values. In Fig. 8, we show the impact of M on $\overline{D_{\max}^{(l)}}$ for RIS 1 and RIS 2 when both RISs are reachable. It is seen that
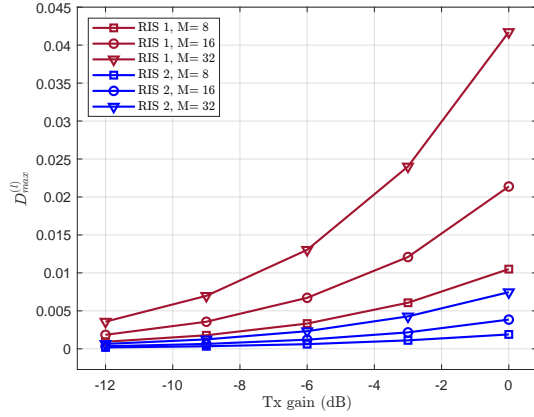
Fig. 8. The impact of M on $\overline{D_{\max}^{(l)}}$ for RIS 1 and RIS 2 in "Both RISs reachable" scenario.
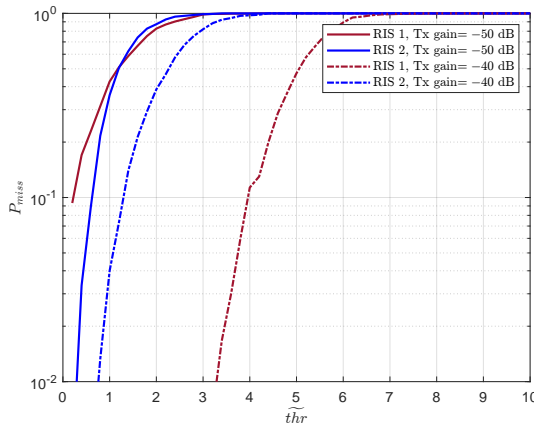

Fig. 9. P_{miss} vs $\widetilde{thr}$ with different Tx gain values in "Both RISs reachable" scenario.
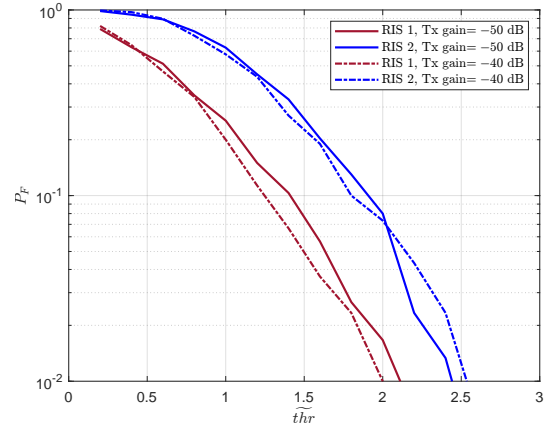

Fig. 10. P_F vs $\widetilde{thr}$ with different Tx gain values in "No RIS reachable" scenario.

RISs with less sensitivity to synchronization issues such as phase and frequency offsets. The proposed method has been tested through practical experiments using RIS hardware and software-defined radio (SDR) modules. Experimental results, including false and miss detection probability metrics, demonstrated the effectiveness of the proposed method in various scenarios with different system settings. Future work will explore optimizing the method for dynamic environments and integrating it with other network functions like beamforming and localization.

increasing M increases $\overline{D_{\max}^{(l)}}$ for both RISs, where doubling M doubles $\overline{D_{\max}^{(l)}}$ for both RISs.

In Fig. 9, the effect of $\widetilde{thr}$ on P_{miss} of RIS 1 and RIS 2 is investigated. The results show that increasing $\widetilde{thr}$ leads to a higher P_{miss} for both RISs. Specifically, when the Tx gain is -50 dB, increasing $\widetilde{thr}$ from 0.6 to 0.8 increases P_{miss} from 0.23 to 0.31 for RIS 1 and from 0.09 to 0.22 for RIS 2. Moreover, increasing the Tx gain decreases the P_{miss} for both RISs. This behavior is evident from Fig. 9 for RIS 2. For example, when $\widetilde{thr}$ is set at 0.8, increasing the Tx gain by 10 dB reduces the P_{miss} for RIS 1 from 0.22 to 0.013.

C. No RIS Reachable Scenario

In the scenario, RIS is removed from the environment, and identification process is performed using Algorithm 1. Then, the effect of $\widetilde{thr}$ on P_F of RIS 1 and RIS 2 is investigated. As seen in Fig. 10, increasing $\widetilde{thr}$ decreased P_F of RIS 1 and RIS 2. For example, when the Tx gain is -50 dB, increasing $\widetilde{thr}$ from 1.4 to 1.8, decreased P_F of RIS 1 from 0.67 to 0.23 and decreased P_F of RIS 2 from 0.27 to 0.1.

V. CONCLUSION

This letter has proposed a novel modulation method for the RIS identification (RIS-ID) process to identify reachable

REFERENCES

[1] Y. Liu et al., "Reconfigurable intelligent surfaces: Principles and opportunities," IEEE Commun. Surveys Tuts., vol. 23, no. 3, pp. 1546–1577, May 2021.
[2] W. Zhang et al., "RIS-assisted self-interference mitigation for in-band full-duplex transceivers," IEEE Trans. Commun., vol. 71, no. 9, pp. 5444–5454, Sep. 2023.
[3] A. Almohamad et al., "Smart and secure wireless communications via reflecting intelligent surfaces: A short survey," IEEE Open J. Commun. Soc., vol. 1, pp. 1442–1456, Sep. 2020.
[4] A. Elzanaty et al., "Reconfigurable intelligent surfaces for localization: Position and orientation error bounds," IEEE Trans. Signal Process., vol. 69, pp. 5386–5402, Aug. 2021.
[5] E. Basar, "Transmission through large intelligent surfaces: A new frontier in wireless communications," in Proc. Eur. Conf. Netw. Commun. (EuCNC), Valencia, Spain, Jun. 2019, pp. 112–117.
[6] W. Tang et al., "Programmable metasurface-based RF chain-free 8PSK wireless transmitter," Electron. Lett., vol. 55, no. 7, pp. 417–420, Apr. 2019.
[7] ——, "Wireless communications with programmable metasurface: New paradigms, opportunities, and challenges on transceiver design," IEEE Wireless Commun., vol. 27, no. 2, pp. 180–187, Apr. 2020.
[8] C. Gaudreauand and A. Chaaban, "Localization by modulated reconfigurable intelligent surfaces," IEEE Commun. Lett., vol. 26, no. 12, pp. 2904–2908, Dec. 2022.
[9] A. Khaleel et al., "A simple detection and identification scheme for reconfigurable intelligent surfaces," arXiv preprint arXiv:2402.12565, Feb. 2024.
[10] S. Abeywickrama et al., "Intelligent reflecting surface: Practical phase shift model and beamforming optimization," IEEE Trans. Commun., vol. 68, no. 9, pp. 5849–5863, Sep. 2020.
[11] J.-B. Gros et al., "RISE-6G RIS environment final model," RISE-6G, Tech. Rep. H2020-ICT-52/RISE-6G/D3.3, Dec. 2022. [Online]. Available: https://rise-6g.eu/Documents/LIVRABLES/RISE-6G_WP3_D3.3_Final_Rev.pdf